Asymmetry of H_β Stark profiles in T-tube hydrogen plasma

S. Djurović, D. Nikolić, and I. Savić
Faculty of Science, Department of Physics, Trg Dositeja Obradovića 4, 21000 Novi Sad, Federal Republic of Serbia and Montenegro

S. Sörge
Bereich Stellaratortheorie, Max-Planck-Institüt für Plasmaphysik, Teilinstitut Greifswald, Wendelsteinstrasse 1, D-17491 Greifswald, Germany

A. V. Demura*
HEPTI, RRC Kurchatov Institute, Kurchatov Square 1, Moscow 123182, Russia
(Received 27 October 2004; published 18 March 2005)

The whole Balmer H_β line profiles are studied in detail experimentally in the T-tube discharge for the wide range of plasma parameters. Besides the common one, two additional parameters are introduced to characterize the asymmetry behavior of the experimental Stark profiles with the reference point chosen in the center of the line. The experimental data are analyzed and benchmarked versus the simple theoretical model based on the effects of microfield nonuniformity and electron impact shifts.

DOI: 10.1103/PhysRevE.71.036407 PACS number(s): 52.70.−m, 32.70.Jz

I. INTRODUCTION

The new extensive observations of the entire Balmer H_β line profiles emitted from T-tube discharges were performed for the following ranges of plasma parameters variation: the electron density $N_e=(2.28-7.30)\times10^{17}$ cm^{-3}, and the electron temperature $T_e=(1.94-3.4)\times10^4$ K.

The measurements of the Balmer H_β Stark profiles were done before numerously as well [1–38] because of fundamental significance for testing the extent of current understanding of diverse physical phenomena of Stark broadening in plasmas versus theoretical approaches validity, and in attempts to improve the potential of diagnostic predictions based on characteristics of its Stark profile, such as a HWHM [39–43]. In time the precise observations revealed a series of interesting physical effects, that each time were quite astonishing since the adopted overall picture seemed complete and clear. In spite of general physical laws established for Stark broadening of hydrogen spectral lines, each line has its own unique features and interrelations of various broadening mechanisms that show up in some distinctive appearance of its Stark line shape being characteristic only for this line. For example, the effect of reduced mass was detected in the H_β profile by the depth of its dip [4–9], and the effects of the dip shift [24,28] and peaks shift [30,37] as well as peaks separation [16,17,26], also were extracted and carefully measured, when it seemed that nothing else has been left. In this context the asymmetry of H_β peaks and red and blue wings was noticed visually a long time ago [1,2] and revisited many times [12,13,24,33].

The latter asymmetry feature was the first one attempted to be explained theoretically by developed up to date approaches [44–64], but in spite of published declarations of its excellent description in [44], then in [45] and at last in [61], it was shown that in fact it did not get the final, consistent and convincing theoretical treatment [64].

In the present experimental study it is shown that there are additional ways to characterize the asymmetry behavior of the whole Stark profile much more thoroughly than it has been done commonly for a long time earlier [1–38], and likely the abilities and predictability of current theoretical approaches are not ready for this challenge yet [44–64]. Basically it occurs that an attentive and careful investigation of comparison of theoretical calculations with experiment, reveals recently large discrepancy between theoretical and experimental asymmetry behavior in the far wings of this spectral line [64]. Therefore at the moment it is appropriate to trace qualitatively this set of new characteristics using, in the basis of theoretical calculations, physically transparent effects in Stark broadening of H_β that may cause its asymmetry. Namely, the effects of ionic microfield nonuniformity [46,48] and the effect of electronic impact shifts [59,60] transformed to give the electronic shifts of individual H_β Stark components (see [46,64]) are considered. Intentionally to underline the qualitative significance of this extensive experimental treatment of the profile asymmetry, the pioneer version of the theory describing the Stark profiles asymmetry in terms of the many-body nonuniform ionic microfield [46] joined with contribution from the electron impact shifts [59,60] is taken as a benchmark to separate, classify and discuss the functional characteristics of the discrepancy between experiment and theoretical predictions. The effects of the Debye electron screening, ion-ion correlations [49–58], and ion dynamics [43,56,57,62,63] are not included. The specific effects of strongly coupled plasmas are also omitted here. The reason for such a choice is that in the present study the "middle" part of the profile is analyzed at detuning from the line center around HWHM, leaving apart the line center with peaks region and the line wings. In this detuning region the other effects causing the Stark profile asymmetry are thought to be insignificant, for example, the line dissolution

*Author to whom correspondence should be addressed. Email address: Alexander.Demura@hepti.kiae.ru

in the strong electric field known to induce the blue asymmetry (see for example [65]).

It is important to underline that the functional asymmetry behavior crucially depends on the choice of the reference point [64]. For the asymmetric profile with a complex structure in the line center with peaks and dips, as in the case of H_β line, the different choices of the reference points on the wavelength scale produce the drastically different dependencies of the asymmetry parameter on the detuning from the reference point [64]. At the same time for such complex asymmetric profiles it is impossible even to introduce the unique definition of the line shift [64]. Therefore in the present investigation the middle point on the wavelength scale at the level of the half intensity of "maximum" is chosen for the position of the reference point. The "maximum" for the line with two peaks in its turn is defined as one half of the sum of intensities in the blue and red maxima. This reference point differs from the position of the unperturbed wavelength of the transition λ_0 and from the position of the dip $\lambda_{\rm dip}$. This important circumstance should be taken into consideration in the analysis of the measured asymmetry.

The H_β line Stark profile obeys, in general for a rather wide range of parameters, the main predictions of Holtsmark theory of quasistatic broadening by ions [46,48,66]. Thus its HWHM is approximately proportional to $N_e^{2/3}$, making from this line the tool to diagnose plasma density. The calculated values of HWHM were defined more accurately accounting for the electron impact broadening [39–42] and providing symmetrical and unshifted Stark profiles [40] that are addressed as the standard theory results (ST). But there are known small deviations versus the square root of reduced mass values of the perturber-radiator pair, indicating the importance of ion dynamics for the dip value determination [2–9,38,43]. It is interesting that the special experiments aimed to find a correlation between ion dynamics and asymmetry of H_β profile did not detect any noticeable interrelation [14]. However, this resume contradicts the results of the full scale calculations for Ly_α showing significant influence of ion dynamics, in the frames of the MMM (model microfield method), on asymmetry of line profile [55–57]. Nevertheless, this contradiction could not be considered as indication of some incorrectness primarily due to the difference in the characteristics of these lines. For example, it is known that the ion dynamics change drastically (by the factor of 2.5) HWHM of Ly_α [67] while the influence of ion dynamics on H_β profile is quite moderate [6–9,14,38].

In the present article the experimental observations of H_β profiles in T-tube plasmas for various values of plasma density and temperatures are compared with simple theoretical description of Stark profiles asymmetry, based on notions of nonuniformity of ion microfield in the quasistatic approximation [46,48] and the electron impact shifts [59,60]. The variety of plasma conditions allows in principle to trace differences between experimental and theoretical results versus the density and temperature, and might give a key for understanding the physical origin of asymmetry.

This article is organized as follows. After the introduction in Sec. I, the description of experimental setup and plasma parameters for which measurements were performed, followed by the substantial analysis of the experimental procedure could be found in Sec. II. Also in Sec. II the set of three asymmetry parameters is defined, exploring various characteristics of profile asymmetry in more detail. Section III is devoted to presentation of the experimental results. The main basics of the theoretical model that is used to benchmark the experimental findings are outlined in Sec. IV. In Sec. V the analysis of experimental results and their comparison with theory is performed and discussed. Section VI summarizes conclusions of the study.

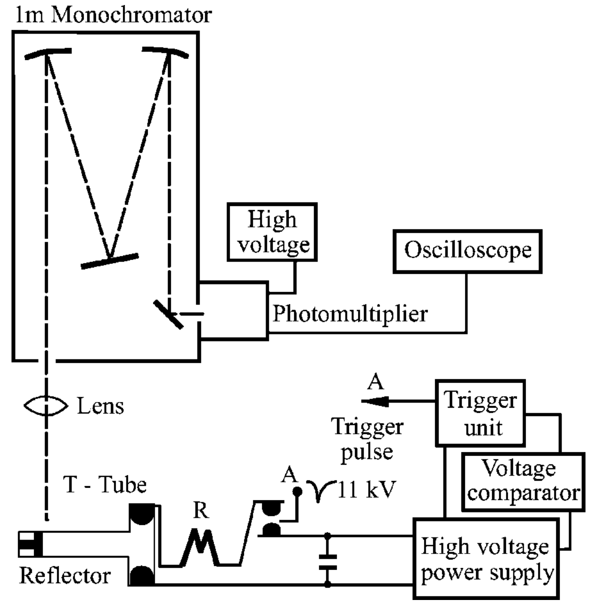

FIG. 1. The experimental setup.

II. EXPERIMENTAL MEASUREMENTS OF H_β STARK PROFILES

A. Plasma source

The plasma source used in this experiment is the small magnetically driven [68], T-shaped shock tube [69], made of glass with the inner diameter of 27 mm. The quartz reflector is placed at 130 mm from the discharge electrodes. The T-tube was energized from the low inductance capacitor bank made of the four parallel connected capacitors, 1 μF each, and charged up to 20 kV. The filling gas was pure hydrogen under the pressure of 300 Pa. The discharge was initiated by the 11 kV trigger pulse via the spark-gap (Fig. 1). Due to the constant flow of hydrogen from behind the reflector to the discharge electrodes, as well as to the activated zeolite molecular vapor trap, the background contamination was negligible. The discharge current was critically damped by the resistor R (Fig. 1) and its duration was 3 μs. This time was equal to the time necessary for the incident shock front to reach the reflector when the filling pressure was 300 Pa. It has been generally accepted [68] that plasmas produced in small electromagnetic T-tubes are quite homogeneous, both radially and axially, behind the reflected shock front.

B. Line shape recording

The experimental setup is schematically presented in Fig. 1. The plasma was observed at the region 4 mm in front of the reflector. The light emitted from T-tube was focused onto the entrance slit of the 1 m monochromator with the inverse linear dispersion of 0.833 nm/mm. The monochromator is equipped with 1200 g/mm grating and with the photomultiplier at the exit slit. The signals from the photomultiplier were led to the oscilloscope. The spectral intensities were measured at 1, 1.5, 2, 2.5, and 3 μs after the reflected shock front passed the point of observation. The H_β line was scanned at close intervals from successive discharges (shot-to-shot technique) over a wavelength band of ±25 nm from the line center. The resulting signal for each of the wavelength setting of the monochromator represents the average of the six shots.

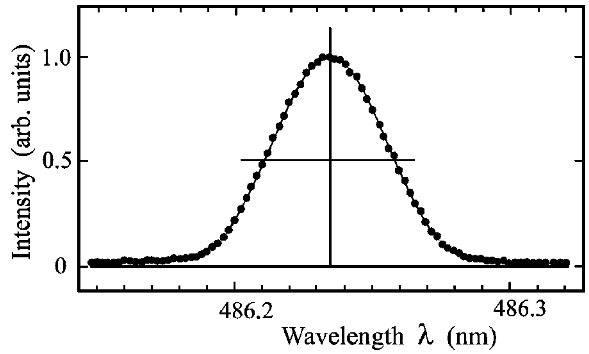

FIG. 2. The recorded instrumental profile of H_β line emitted from low pressure Geissler tube.

C. Plasma diagnostics

The electron densities N_e ranging from 2.28×10^{17} cm^{-3} to 7.30×10^{17} cm^{-3} have been determined from the Stark widths of the H_β line profiles. The N_e deduction was performed with the help of the theoretically calculated data from [39,40]. The estimated uncertainties of the electron densities do not exceed ±9%.

The electron temperatures T_e, ranging from 19400 K to 34000 K, have been determined from the line-to-continuum ratios of the H_β line [39]. The uncertainties for the electron temperature measurements are between ±8% and ±15% from the lower to the higher values. The existence of the local thermodynamic equilibrium was checked.

D. Processing of experimental profile

In the recording procedure the signal intensities are normalized to the spectral sensitivity of the optical system. It has to be done, since the experimental profiles of H_β line are very broad, several tens of nanometers. In the next step, the contribution of the adjacent H_α and H_γ lines is eliminated. The influence of H_β line is practically negligible while the influence of H_γ line to the blue wing of H_β line is substantial. The red wing of H_γ line raises the blue wing of H_β line at the detuning from the line center of about the two halfwidths. For electron densities from 2.28×10^{17} cm^{-3} to 7.3×10^{17} cm^{-3} this contribution ranges from 20% to 57%, respectively. The continuum level is determined in assumption that the far line wings could be described by the asymptotic formula $I\propto(\Delta\lambda)^{-5/2}$ [39].

In principle, the measurement of the intensity of radiation from pulsed sources, such as electromagnetic shock T-tube, gives scattered points due to a very short observation time and experiences certain irreproducibility of plasma parameters. This makes the detailed analysis of the H_β line profile rather difficult especially in the region of the profile maximums. A substantial part of the uncertainties in determination of various parameters from the experimental profile arises just due to scattered points. The point scattering is decreased to the optimal level by taking each point of the recorded profile as the average value of six measurements. Therefore, each point has its own error bar entering the least square fit. The corresponding fitting curves through the given profile provide the optimal values for the intensities or positions. The same curves enable to deduct the halfwidth of H_β line profile as well as the asymmetry parameters.

E. Analysis of necessary experimental conditions for asymmetry measurement

Before determining the asymmetry parameters from experimentally recorded profiles of H_β line, it is necessary to eliminate from the profile the trivial asymmetry. The experimental trivial asymmetry sources are instrumental asymmetry, line self-absorption, plasma inhomogeneity, emitter motion along the line of observation, and overlapping of neighboring spectral lines.

The instrumental asymmetry is simply checked using a spectral line emitted from a low-pressure source. The line emitted under these conditions is symmetric and practically only naturally broadened. The example of the instrumental profile of H_β line, emitted from Geissler tube is presented in Fig. 2. The profile is symmetric meaning that the monochromator and the optical system at large do not introduce any additional asymmetry.

The emitter motion along the observation line, i.e., Doppler effect also should not be the asymmetry source. The Doppler halfwidth is only about 0.6% of Stark halfwidth of H_β line in the present experimental conditions. The emitter distribution over thermal velocities in the present experimental conditions do not differ noticeably from the Maxwellian isotropic distribution. There exists only the motion of the shock wave front in T-tube, i.e., the motion of plasma as a whole with respect to the observation system. In this case only the transverse Doppler effect might be remarkable. This effect is however negligible with respect to the longitudinal one. In the most unfavorable case, for the velocity of the gas behind the shock wave front equal to 1×10^{6} cm/s [36], the wavelength change due to this effect equals only 3×10^{-7} nm. So, this effect also could be discarded as a possible source of the trivial asymmetry. The check of self-absorption was performed in earlier works [3,69], indicating that it does not exceed 2%. The theoretical estimates [39,42] show that for considered parameters the radiation self-absorption of H_β must be below 4%. Thus deviations in intensity due to self-absorption are within the limits of both theoretical and experimental errors and could be neglected during the processing and analysis of the experimental data. Moreover, the emitted radiation can in principle be absorbed in the colder layer close to the wall of the discharge tube. It was shown in [22] that this effect could decrease the intensity of the spectral line for about 2.5%, if the cold layer width is about 1 mm. However, as it was demonstrated in [18] the width of the cold layer within first 2.5 μs, after the passage of the reflected front of the shock wave through the observation point, is much smaller than 1 mm and negligible, but rises linearly with time. Only after first 2.5 μs it raises faster than linear, yet after 5 μs it is still smaller than 1 mm. The similar conclusions are valid for the influence of the cold layer to the intensity of the continuum radiation [23].

Besides the absorption, the emission from the cold layer can also occur. Such emitted profiles of H_β line are, however, substantially narrower than the profiles emitted from hot plasma. They might have some effect in the later moments of the plasma lifetime, but only in the central part of the profile. The emissivity of the cold layer is considered to be much smaller than the radiation from hot plasmas due to its much lesser radiation volume as well. Moreover, the central part of the profile is not the object of the present experimental study. Thus, for the particular experimental conditions and setting, the influence of the cold layer could be discarded as well.

During the analysis of the local thermodynamical equilibrium conditions it was possible to verify that according to the calculated diffusion length, plasma during the observation time of 3 μs is homogeneous. As the indicator of plasma homogeneity it is possible to use the ratio $\Delta\lambda_p/\Delta\lambda_{1/2}$ [7,8], where $\Delta\lambda_p$ denotes the separation between the red and the blue maximums of H_β line profile. The theoretical calculations in [40] give the value 0.35, and 0.37 in VCS [41]. The experimental measurements, performed in [7,8] and [17], report for this ratio correspondingly the values 0.36 and 0.354 in good agreement with theoretical calculations. Thus the results obtained in the present experiment, ranged between 0.35 and 0.36, could be a confirmation of the plasma homogeneity. It should be pointed out, that a very small temperature gradient [69], as well as very small electron density gradient [21], exist along the tube axis. But the gradients of temperature and electron density along the radius, i.e., the observation direction are practically negligible [69].

Since the plasma within the T-tube is nonstationary mobile, one should take into account the possible turbulence effects. The observable turbulence is noticed for the incident wave but it practically disappears in the reflected wave [25]. This means that plasma turbulence can be eliminated as a possible trivial source of the experimental profile asymmetry.

F. Treatment of experimental profile and introduction of asymmetry parameters

Apart from above mentioned experimental sources of trivial asymmetry, proper treatment of the experimental data is also important. It was already mentioned that H_β line emitted from plasma possesses more or less asymmetric profile, which is also shifted with respect to the wavelength that would be emitted by an isolated and motionless atom. The

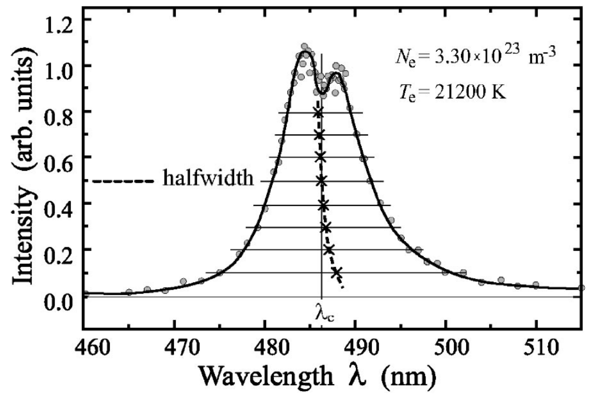

FIG. 3. The demonstration of the asymmetry in the experimental profile of H_β line.

blue maximum in an experimental profile is higher than the red one, while the red wing is always higher than the blue one. This was observed in a series of experimental studies (see for example [1–19]), and confirmed as well in the present experiment.

Often under the "H_β profile asymmetry" the inequality of the two maxima of this line is meant, e.g. [16,45,61]. This asymmetry was noticed already in the thirties of the preceding century [1]. In this paper the wider notion of asymmetry is used to describe the whole shape of the H_β line profile as in [64]. Figure 3 shows the H_β line experimental profile asymmetry for the electron density 3.3×10^{17} cm^{-3} and electron temperature 21200 K. The middle points of the separation between blue and red wings are denoted at various heights with respect to the maximal intensity. These points are connected by the dashed curve, which clearly indicates the asymmetry of the profile.

Here the "line center point" λ_C designates the position of the middle point at the half maximum (HM) height of the profile, and will be used in the following as the reference point instead of the position of the unperturbed line wavelength λ_0 or position of the dip λ_{dip}. The HM is nothing else but one half of the maximal intensity I_0 defined as the mean value of the blue and red maximums.

Astonishingly there are only few works attempted to conduct the analysis of the whole H_β line profile asymmetry [4,64], according to our knowledge. The profile asymmetry can be analyzed in terms of the corresponding parameters, which can be defined in various ways [64]. In this work the three parameters to estimate the asymmetry are used. The first parameter of asymmetry is determined conventionally by the expression

$$A_1(\Delta\lambda) = \frac{I_R(\Delta\lambda) - I_B(\Delta\lambda)}{I_R(\Delta\lambda) + I_B(\Delta\lambda)}. \tag{1}$$

The parameter $A_1(\Delta\lambda)$ is common and does not need any special introduction, but it is necessary to note that in the present definition it does not contain the factor 2 in the numerator and for the reference point the line center λ_C is taken instead of λ_0. As already pointed out, this choice of the reference point could drastically change the functional behavior of $A_1(\Delta\lambda)$ when compared with the reference point at the

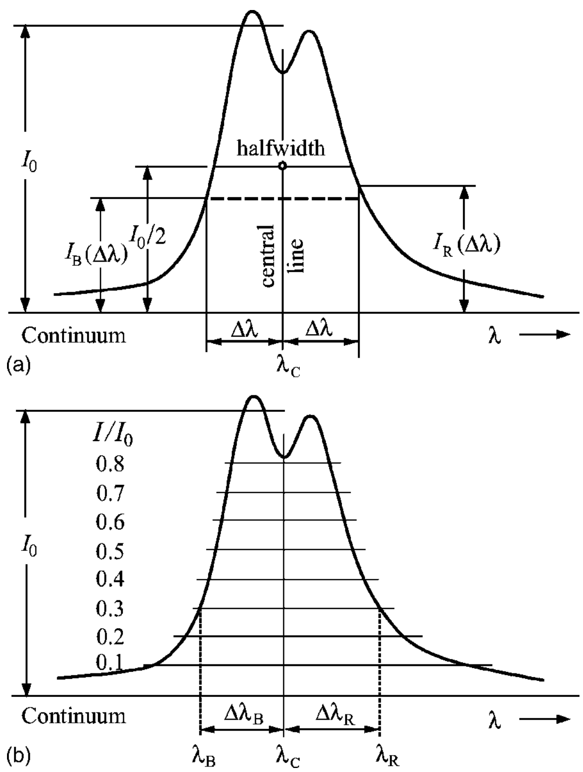

FIG. 4. The illustration of the procedure used for determination of asymmetry features. (a) Description of quantities entering in parameter A_1 evaluation. (b) The intensity levels at which the values of parameters A_2 and A_3 were sampled.

unperturbed line position λ_0 [48,64]. The procedure for determining the parameter $A_1(\Delta\lambda)$ is demonstrated in Fig. 4(a). There $I_R(\Delta\lambda)$ and $I_B(\Delta\lambda)$ denote the intensities in the red and the blue sides of the profile measured at the equal distances $\Delta\lambda$ with respect to the chosen reference point λ_C—"the line center" (see Figs. 3 and 4).

The second asymmetry parameter $A_2(\varphi(\Delta\lambda))$ is introduced in fact as the transcendent function of the intensity normalized profile $\varphi(\Delta\lambda)=I(\Delta\lambda)/I_0$. It is defined by the equation

$$A_2(\varphi(\Delta\lambda)) = \frac{\Delta\lambda_R[\varphi(\Delta\lambda)] - \Delta\lambda_B[\varphi(\Delta\lambda)]}{\Delta\lambda_R[\varphi(\Delta\lambda)] + \Delta\lambda_B[\varphi(\Delta\lambda)]}, \qquad (2)$$

in which the values of $\Delta\lambda_{R,B}[\varphi(\Delta\lambda)]$ are determined from the equality

$$\varphi(\Delta\lambda_R) = \varphi(\Delta\lambda_B). \qquad (3)$$

The determination of the parameter $A_2(\varphi(\Delta\lambda))$ is illustrated in Fig. 4(b). The $\Delta\lambda_B$ and $\Delta\lambda_R$ denote the distances on the blue and red sides of the profile from the central line λ_C, measured at the various intensity levels.

The third asymmetry parameter $A_3(\varphi(\Delta\lambda))$ is defined additionally to the second one, and determines the one half of the difference between $\Delta\lambda_R$ and $\Delta\lambda_B$

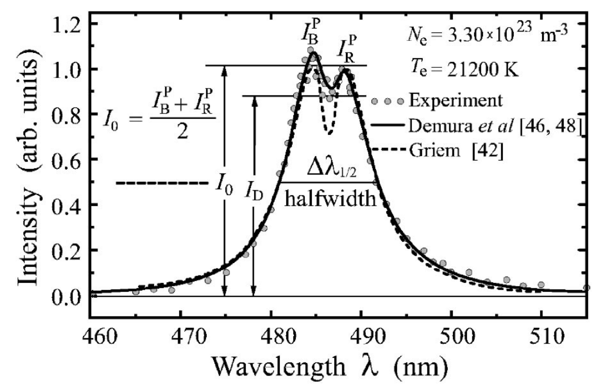

FIG. 5. The comparison of the experimental profile of H_β line with corresponding theoretical profiles.

$$A_3(\varphi(\Delta\lambda)) = \frac{\Delta\lambda_R[\varphi(\Delta\lambda)] - \Delta\lambda_B[\varphi(\Delta\lambda)]}{2}. \qquad (4)$$

This parameter $A_3(\varphi(\Delta\lambda))$ is not quite new. Indeed, the asymmetry in the wings was evaluated previously as well [70], using Eq. (4). In the wings it was possible to perform expansion of Eq. (4) and express $A_3(\varphi(\Delta\lambda))$ in terms of $\Delta\lambda$ [46]. But with the definition of reference frame adopted here the functional behavior of $A_3(\varphi(\Delta\lambda))$ might be quite different. Moreover, in [48] it was shown that in the wings $A_3(\varphi(\Delta\lambda))$ in terms of $\Delta\lambda$ in fact can be expressed as the limit of $A_1(\Delta\lambda)$ at large $\Delta\lambda$. The third asymmetry parameter represents the distance of the middle point at some line intensity level ($I/I_0=0.1, 0.2, \ldots, 0.8$) from the central line, as shown in Fig. 4(b). The parameters A_1 and A_2 are dimensionless while the parameter A_3 is expressed in the units of wavelength.

III. EXPERIMENTAL RESULTS

A. Overall analysis of experimental profile: halfwidth, peaks, and dip

The example of the overall comparison of the experimental profile and the normalized to unity theoretical profiles of H_β line [42,46,48] for the corresponding electron density and temperature is given in the Fig. 5. The halfwidth of each theoretical profile was set to the value of the experimental line halfwidth. Hence the slightly deviating values of electron densities are read for the different theoretical approaches [42,46,48], see Sec. IV, noting that VCS [41] does not contain tabulation for electron densities higher than 1×10^{17} cm^{-3}.

Obviously, the symmetric ST profile [42] cannot describe the central structure of the experimental profile. Besides that it gives a much larger dip [42] than in the experiment. The theoretical approach in [46,48], contrary to ST [42], gives different intensities of two maxima, but with somewhat smaller dip between them. These deviations could be described in terms of the following coefficient ΔD (similar to [6]):

$$\Delta D = \frac{I_0 - I_D}{I_0} \times 100\,\%, \qquad (5)$$

expressing the relation between the intensities of the maximum I_0 and the dip minimum I_D in percents. In the case of experimental profiles and in [46,48] the intensity of the maximum I_0 represents the average value of the blue I_B and red I_R maxima. The value of the coefficient ΔD for the experimental profile in the Fig. 5 is 14%, in [42] it is 30%, and in [46,48] it is 10.7%.

At the same time the latter analysis of the dip is oversimplified, first of all with respect to the neglected ion dynamics [11] and fine structure [15] effects. Moreover, the central dip depth in experimental profiles of H_β line recorded in the shock electromagnetic tube may be influenced also by the emission from the colder layers close to the walls of the discharge tube [15]. If this occurs then, in principle, the central part of H_β line might be used for testing plasma homogeneity [7,8]. It is also well established that the dip and peaks experience shifts depending on density and temperature [4,9,24,28,30,37]. Thus it is obvious that the treatment of the central part of H_β represents a rather complex problem in the case of T-tube plasmas experimental observations.

On the other hand, it should be noted that the accuracy of the density diagnostics from the measurement of the line halfwidth in fact is limited by the existence of the characteristic peaks of H_β profile and due to the continuum level determination problem. That is why the other proposed methods [20,32,34,71] of the density diagnostics are based, for example, on fitting exclusively the experimental line wings [20,32] or areas under maxima [32,72] to VCS profiles [41]. However, it was shown [34,71] that methods using the whole experimental profiles for the χ^2-minimization fitting provide by about 10% the lesser density values than those determined from the halfwidth. In general, fitting only the parts of experimental profiles could lead to higher electron densities [34,71] than the real ones. Interestingly, the output of these methods depends on the direction of fitting procedure implementation with respect to the line center [34,71]. It turned out that fitting is more successful if it started from the wings towards line center. Inconsistency of the fitting output might be a result of insufficiently refined theoretical models and profiles that lack to reproduce the real interrelations of various physical effects [39]. For example, in the case of VCS profiles, which in the range of low density exhibit three times larger dip than in the experiment, this leads to the fitting output of lower electron densities [34]. That is why the fitting procedure often was used avoiding the central region of the line (see [34,71]).

However, for the electron densities within the range 10^{16}–10^{17} cm^{-3} the line halfwidth is highly sensitive to Stark broadening, while the effects of ion dynamics are small. In this case, the halfwidth method is rather reliable for the determination of electron density with relative error of about 5% [32]. Thus, according to results of the previous section, the estimated accuracy of the experimental profiles in the context of attributing to them the certain density and temperature values varies from ±13% to ±20%. The best agreement of all three profiles in the Fig. 5 is in the region of the line halfwidth. The whole experimental profile of H_β line possesses certain asymmetry which is mostly expressed in the region of maxima and in the line wings. The similar properties are manifested by the theoretical profiles in [46,48].

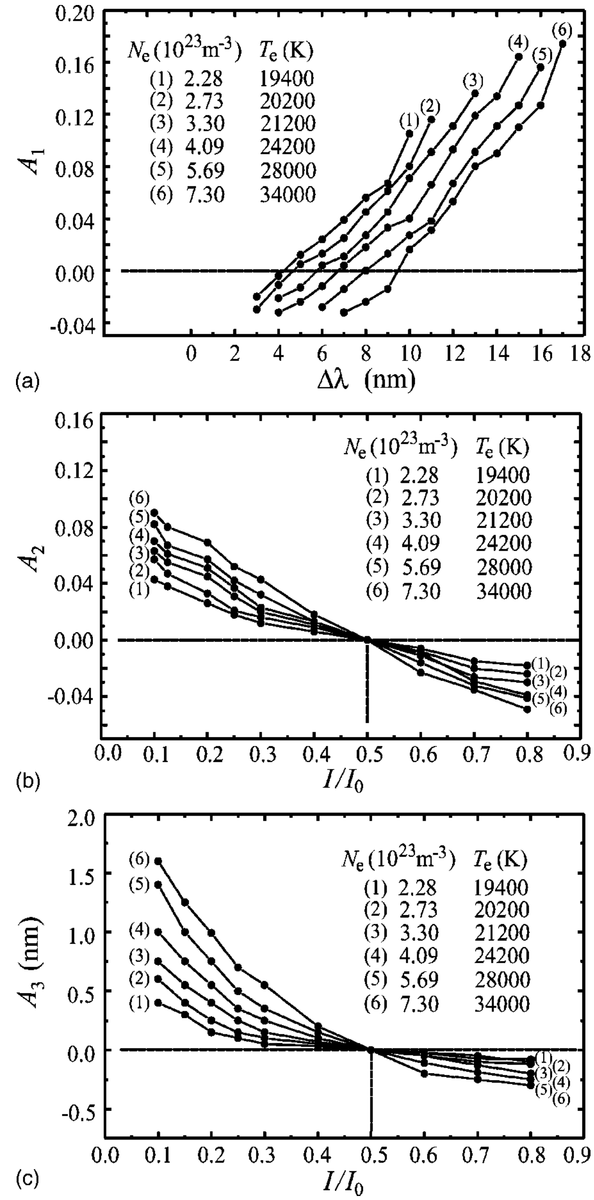

FIG. 6. The experimental values of asymmetry parameters obtained in this work for indicated plasma conditions.

B. Experimental asymmetry parameters

The experimentally determined values of asymmetry parameters of H_β line, $A_1(\Delta\lambda)$, $A_2(\varphi(\Delta\lambda))$, and $A_3(\varphi(\Delta\lambda))$, are presented in Fig. 6 as a set of curves corresponding to the different density magnitude, and are indicated by numbers within brackets. The parameter $A_1(\Delta\lambda)$ is plotted in terms of the distance $\Delta\lambda$ from the line center λ_C, and the other two parameters are given in terms of the ratio of the height at which the measurement is performed and the maximal intensity $I(\Delta\lambda)/I_0=\varphi(\Delta\lambda)$, thus being transcendent functions of $\Delta\lambda$ through the values of normalized profile $\varphi(\Delta\lambda)$. All parameters by definition vanish within the range of the line halfwidth since they are calculated with respect to the central line λ_C (see Fig. 3 and Fig. 4). The measured values of the mentioned parameters unambiguously indicate the existence of the asymmetry of experimental profiles of H_β line. The asymmetry parameters measured at the upper half of the profile, i.e., above the halfwidth region of H_β line are negative. This implies that the "minus" sign is valid for the values $\Delta\lambda<\Delta\lambda_{1/2}/2$ and $I/I_0>0.5$, if to exclude as it was arranged above the region of maxima (see Fig. 3). The functional dependence of the experimental asymmetry parameter $A_1(\Delta\lambda)$ significantly differs from the known common functional behavior [48] as it was warned earlier [64] due to the difference in the definition of the reference point λ_C instead of more common λ_0 or λ_{dip}.

While examining the functional behavior of asymmetry parameters it should not be forgotten that the each fixed electron density value corresponds to the certain value of electron temperature and thus it is unlikely reasonable to seek a simple proportionality between the curves in the set, corresponding to the different density values, although the similarity of the functional behavior is visually obvious. Furthermore, the density and temperature dependence of the normalized profiles is rather complicated and not linear. Therefore, with respect to the subtle profile features such as asymmetry parameters, it should be kept in mind that it is difficult to achieve sufficient overall experimental accuracy.

IV. THEORETICAL MODEL

The theoretical approach shortly outlined here is based on the description of broadening by plasma ions in the frames of quasistatic approximation [46] and the broadening by electrons in the frames of the impact approximation [46,73]. Namely, the difference in the characteristic time scales of ions and electrons movement preserves from cancellation the contribution to broadening due to the effects of microfield nonuniformity on atomic scale, i.e., due to the expansion of the interaction potential to the second order with respect to the ratio of the characteristic atomic scale n^2a_0 (n is principal quantum number; a_0 is the Bohr radius) to the mean distance R_0 between the radiator and the perturbing particles with the opposite charge. It is obvious, if taken on the same foot, such contributions would practically cancel each other [42,46,48,53].

In order to tackle the nonuniformity of ion microfield, the joint distribution function of the ion microfield strength vector $\vec{F}$ and the linearly independent components of its nonuniformity tensor $\{\partial F_i/\partial x_j\}$ is constructed [46,48–58]. However, such a function of the eight linearly independent variables could not be evaluated for the aims of realistic calculations [46,48–58]. But if to use the perturbation expansion to the contour in the first order of the perturbation parameter $\varepsilon=n^2a_0/R_0\ll 1$, then it is possible to express the solution through the first moments of the nonuniformity tensor, which drastically simplify the calculations [46]. Moreover, it is possible to obtain in the closed form the expressions for these first moments in terms of the universal functions, directly related to the generation function of the microfield distributions obtained in various approaches [46,48–56].

In this section the parabolic basis of the quantum states of hydrogen atom is used as in [46,48]. Then the each Stark sublevel is characterized by the set of quantum numbers $\{n,n_1,n_2,m\}$, where $n_{1,2}$ are parabolic quantum numbers and m is the magnetic quantum number. In the diagonal approximation for the electron collision operator [46,48] the Stark profile of hydrogen spectral line $I_{nn'}(\Delta\omega)$ describing the line shape of the radiative transition $n\to n'$ may be represented as a sum of the profiles $I_{(n\alpha),(n'\beta)}(\Delta\omega)$ of the individual Stark components, corresponding to the transition between the Stark sublevel α of the upper level n and the Stark sublevel β of the lower level n'

$$I_{nn'}(\Delta\omega)=\sum_{\alpha\beta} I_{(n\alpha),(n'\beta)}(\Delta\omega), \tag{6}$$

where $\Delta\omega=\omega-\omega_0$, ω is the frequency of radiation and ω_0 is unperturbed frequency of the transition $n\to n'$. Then for the sum of the profiles of the two symmetrical individual Stark components designated by the index k and $-k$, for which the constant of linear Stark effect $C_k^{(1)}$ is proportional to $\Delta_k^d=[n(n_1^\alpha-n_2^\alpha)-n'(n_1^\beta-n_2^\beta)]$, that obeys the relation $\Delta_k^d=-\Delta_{-k}^d$, it is possible to write the following expressions that include effects of microfield nonuniformity [46,48,53,64] and the electron impact widths γ_k and shifts $d_k^{(e)}$

$$I_{k,-k}(\Delta\omega)=I_k(\Delta\omega)+I_{-k}(\Delta\omega), \tag{7}$$

$$I_{k,-k}(\Delta\omega)=\frac{I_k^{(0)}}{\pi\left(\sum_k I_k^{(0)}\right)}\int_0^\infty dbW(b)[L_k(\Delta\omega;b)+L_{-k}(\Delta\omega;b)], \tag{8}$$

$$L_k(\Delta\omega;b)=\gamma_k L_k^{(0)}(\Delta\omega;b)+L_k^{(I)}(\Delta\omega;b)+L_k^{(\Delta)}(\Delta\omega;b)+L_k^{(\gamma)}(\Delta\omega;b), \tag{9}$$

$$L_k^{(0)}(\Delta\omega;b)=[(\Delta\omega-C_k^{(1)}b-C_k^{(2)}b^2-d_k^{(e)})^2+\gamma_k^2]^{-1}, \tag{10}$$

$$L_k^{(I)}(\Delta\omega;b)=L_k^{(I,q)}(\Delta\omega;b)+L_k^{(I,qs)}(\Delta\omega;b), \tag{11}$$

$$L_k^{(\Delta)}(\Delta\omega;b)=L_k^{(\Delta,q)}(\Delta\omega;b), \tag{12}$$

$$L_k^{(I,q)}(\Delta\omega;b)=L_k^{(0)}(\Delta\omega;b)[\delta_k^{(q)}\chi_{\text{D}}(b)+\delta_k^{(q0)}\chi_{\text{D0}}(b)], \tag{13}$$

$$L_k^{(\Delta,q)}(\Delta\omega;b)=L_k^{(0)}(\Delta\omega;b)[q_k^{(q)}\Lambda_{\text{D}}(b)+q_k^{(q0)}\Lambda_{\text{D0}}(b)], \tag{14}$$

$$L_k^{(\gamma)}(\Delta\omega;b)=L_k^{(0)}(\Delta\omega;b)G_k^{(\gamma)}(\Delta\omega;b)[P_k^{(q)}\Lambda_{\text{D}}(b)+P_k^{(q0)}\Lambda_{\text{D0}}(b)], \tag{15}$$

$$G_k^{(\gamma)}(\Delta\omega;b)=1-2\gamma_k^2[L_k^{(0)}(\Delta\omega;b)]^2, \tag{16}$$

$$L_k^{(I,qs)}(\Delta\omega;b) = L_k^{(0)}(\Delta\omega;b)\delta_k^{(qs)}b. \qquad (17)$$

Here $I_k^{(0)}$ is the unperturbed intensity of the kth Stark component, $b=F/F_0$ is the reduced value of ion microfield, where $F_0=2\pi(4/15)^{2/3}eZ_pN_i^{2/3}$, e is the electron charge, eZ_p is the charge of the perturbing ions, N_i is the density of the perturbing ions, and $W(b)$ is the ion microfield distribution function. The universal functions $\chi_{D,D0}(b)$ and $\Lambda_{D,D0}(b)$ describe the Stark profile asymmetry due to the quadrupole and polarization interactions. They were first defined in [50,51] by the expressions

$$\Lambda_{D,D0}(b) = \frac{1}{b}[W(b)B_{D,D0}(b)],$$

$$\chi_{D,D0}(b) = -\frac{d}{db}[W(b)B_{D,D0}(b)]. \qquad (18)$$

The universal functions $B_D(b)$ and $B_{D0}(b)$ were also introduced and constructed in the frames of the Baranger-Mozer cluster expansion approach for the arbitrary composition of plasma ions in the Debye approximation in [50,51] (compare with [52]). They were generalized for the arbitrary type of correlation and screening functions in [53,54], studied for various plasma ionization compositions and tabulated using as Baranger-Mozer cluster expansion as Monte Carlo simulations for various values of the ratio $a=R_0/R_{De}$ and the ionic plasma coupling parameters $\Gamma_i=e^2Z_pZ_r/(R_{0i}T_i)$. Here R_{De} stands for electron Debye radius, while eZ_p and eZ_r are the charges of the perturbing and radiating ions correspondingly, with R_{0i} as mean distance between ions and T_i being the ionic temperature [53,54]. The function $B_D(b)$ corresponds to the quadrupolar part and of the first moments of the microfield nonuniformity tensor, while the function $B_{D0}(b)$ corresponds to the scalar (polarization) part of the same first moments with account of screening by electrons, ion-ion correlations and polarization effects (see [50,51,53–58]).

The written above expressions are obtained as the perturbation expansion for the line profile and contain the following corrections of the Stark components subprofiles due to the ion microfield nonuniformity: (a) corrections to the intensity values, proportional to $\delta_k^{(q,q0)}$; (b) corrections to the frequencies, proportional to $q_k^{(q,q0)}$; (c) corrections to the electron impact widths, proportional to $P_k^{(q,q0)}$. These corrections are proportional to the dimensionless parameter $a_0N_i^{1/3}$, and can be expressed through corresponding matrix elements between parabolic quantum states [46,48,53,56].

The asymmetry features of the contour arise from the following symmetry relations with respect to the red $C_{-k}^{(1)} < 0$ $(-k)$ and blue $C_k^{(1)} > 0$ (k) shifted Stark components (see [46,48,53,56])

$$C_k^{(1)} = -C_{-k}^{(1)},$$

$$\delta_k^{(q)} = -\delta_{-k}^{(q)}, \quad q_k^{(q)} = -q_{-k}^{(q)}, \quad P_k^{(q)} = -P_{-k}^{(q)}, \qquad (19)$$

$$\delta_k^{(q0)} = -\delta_{-k}^{(q0)}, \quad q_k^{(q0)} = -q_{-k}^{(q0)}, \quad P_k^{(q0)} = -P_{-k}^{(q0)}.$$

In all expressions the subscript k designates the certain set of quantum numbers, which uniquely determine the Stark component of the line. The superscript q designates quadrupole effects and the superscript $q0$—the polarization effects arising due to the scalar part of the microfield nonuniformity tensor. The $C_k^{(1)}$ is the constant of the linear Stark effect and $C_k^{(2)}$ is the constant of the quadratic Stark effect of the kth Stark component [74]. The first one is proportional to the $(a_0N_i^{1/3})^2$, while the second one to the $(a_0N_i^{1/3})^4$ [46,48,53,56,64]. The corrections to intensity due to the quadratic Stark effect are defined by $\delta_k^{(qs)}$ that is proportional to $(a_0N_i^{1/3})^2$ [53]. The quadratic Stark constants obey the following symmetry relations [74]

$$C_k^{(2)} = C_{-k}^{(2)}, \quad \delta_k^{(qs)} = -\delta_{-k}^{(qs)}, \qquad (20)$$

that obviously also generate some asymmetry in the Stark profile [74]. In fact the corrections due to the quadratic Stark effect are introduced here to demonstrate once more that it is necessary to consider simultaneously the corrections to the energy (the well known quadratic Stark shift) and to the intensity [46,48].

Very often the latter corrections were omitted that led to erroneous non-self-consistent results in the frames of just only the quadratic Stark consideration [49,61,63]. But the real situation is much more complex, and demands to consider at the same time all corrections of the same order. Namely, besides the already entered quadratic Stark effect corrections of the first order, it should be considered additionally: the octupole and the second order quadrupole corrections to the energy, the octupole and the second order quadrupole and the second order quadratic Stark corrections to the intensity (see first [46,48]), that in the case of many-body microfield consideration was not resolved up to now, since the derivation of moments of the more complex joint distribution functions is required [46,48,53]. For brevity the lengthy analytical expressions for various C, δ, q and P factors expressed through the parabolic quantum numbers are omitted here, but they are available in [53,56].

In the present calculations the electronic impact shifts $d_k^{(e)}$ consists from two parts—symmetrical $d_k^{(es)}$, and antisymmetrical $d_k^{(ea)}$

$$d_k^{(e)} = d_k^{(es)} + d_k^{(ea)}, \quad d_k^{(es)} = -d_{-k}^{(es)}, \quad d_k^{(ea)} = d_{-k}^{(ea)}. \qquad (21)$$

The antisymmetrical part $d_k^{(ea)}$ is due to recoil effects at the isoenergetic surface with the fixed principal quantum number, that are beyond the classical trajectory impact approximation, and due to the contribution from the inelastic collisions inducing transitions between the nearby levels with principal quantum numbers $n=n\pm1$ [60], that in its turn is beyond the no quenching approximation. This part mainly causes the red shift of the Stark components and the line as a whole. The similar contributions to the impact width are conventionally considered as negligible [42]. The values of the antisymmetrical shifts were provided in accordance with Green's function approach [59,60] and transformed from the initially spherical basis to the parabolic one employed in the present formulation. The contribution from the recoil effects is made possible due to the fully quantum-mechanical formulation of Green's function method [59]. The rather weak dependence of $d_k^{(ea)}$ on $\Delta\omega$ is neglected (see [60,61]). This is usually considered as the condition of the ST conventional impact approximation, but it is not so, because all contribution to the antisymmetrical part arises in fact due to going beyond its limits [59,60]. This approach does not have problems with "cutoffs" of the impact parameter and is thought to give more accurate account for the strong collisions, than so drastically influenced by "cutoffs" the semiclassical electron impact shift values [75–77]. The term "impact" here means "collisional" and not "in the impact approximation," although the Green's function approach is assumed to take account of many-body effects of electron-atom interaction being in virtue the statistical approach operating with the plasma dielectric function [59]. Thus in the present model the approaches for the calculations of the widths and the shifts of the Stark components are different, but nevertheless it could not be considered as any inconsistency.

In the present paper the simplified results of the outlined theory are intentionally used, where the effects of Debye screening by electrons, ion-ion correlations and polarization effects were neglected. Then the microfield distribution function may be either Holtsmark distribution $H(b)$ or the nearest neighbor distribution $W_{\mathrm{N}}(b)$, and the terms in the general expressions [see Eqs. (13)–(15)], containing factors with superscripts $(q0)$ are omitted.

As it was already stated this approach significantly differs from the ST [39,40,42] by the description of asymmetry features, but neglects the off-diagonal matrix elements of the electron broadening operator in the parabolic representation, because they prevent to reduce the problem in the frames of the perturbation approach to the moments of the joint distribution function. This causes the somewhat increasing of the HWHM of the present profile with respect to ST due to the absence of the inversion procedure for the resolvent matrix, under condition that the same microfield distribution function is used in both cases [46,48,53]. Here the area normalized Stark profiles with the parabolic electron impact widths are calculated using the Holtsmark microfield distribution $H(b)$ that is somewhat wider than the Hooper distribution function [78] used in the ST calculations. So, it is not astonishing that the HWHM of the resultant profile is a bit wider than the ST one as it could be seen from comparison of the experimental profile with ST and the profile, calculated along with [46,48], already presented in Fig. 5. The reason for that is the wider microfield distribution function and the absence of resolvent matrix inversion. It is also seen the lesser dip depth of H_β in the present calculations with respect to ST. If the same microfield distribution function is used then this fact counts in favor of the fact that the effective electron broadening in ST is narrower than in the present calculations. However, it is known that the ST electronic impact operators omit the interference terms, important for the decreasing reduction in the values of the electron impact widths, while in the used here parabolic electron impact operator they are present [46,48]. So, those spherical impact widths should be wider than parabolic ones, but it occurs the opposite. So, the difference seems to be (additionally to resolvent matrix inversion) in the implemented in ST semiempirical procedure for cutoffs applied for the integration over impact parameters, that in particular, may approximately take account of incomplete collisions and thus the electron impact widths start to depend on the detuning from the line center in the line wings [40]. The fact that the cutoff procedure is the source of the difference between the parabolic electron impact widths of the individual Stark components accepted here and the spherical electron impact widths in the ST was established in earlier works during the comparison of the results of kinetic theory of broadening [79] with the simulations performed in [80]. However, the individual parabolic electron impact widths more properly correspond to the solution when the wave functions are quantized along the ion microfield direction [73]. So, in fact the resolution of question which approach is more correct for the description of the electron density values needs the special study and should be determined by the independent diagnostic methods because the HWHM is an integral function of rather numerous parameters. This is quite a difficult task that is beyond the scope of the present work. However, returning to the recipes of semi-empirical cutoff procedure in ST it should be underlined that they were elaborated during certain efforts and time to accomplish the match between ST and the set of experimental profiles accumulated to date of the ST formulation, but since then the various aspects of the theory of electron broadening were considerably remade from the response to detected new discrepancies between predictions of ST theory and experiment [81].

The discussed sources of deviations however may be practically removed. Indeed, first of all the procedure of semiempirical cutoffs might be introduced in any formulation of the impact approximation and in particular in used here parabolic representation of the electron impact broadening operator.

Secondly, to account for nondiagonal matrix elements of the electron impact broadening operator one has to use the Hamiltonian and thus resolvent averaged over components of the microfield nonuniformity tensor. This approximation allows avoiding the perturbation expansion in the contour, although statistically it is less justified. The further step then consists in the inverting matrix of resolvent during which in principal the new linear combinations of wave functions are introduced in the calculation of the dipole matrix elements, describing Stark intensities. These new wave functions diagonalize resolvent with respect to: (a) the electron broadening operator; (b) the linear Stark effect; (c) the quadrupole and polarization effects expressed through the first moments of the microfield non-uniformity tensor; (d) the quadratic Stark effects contribution [46,48,53,56]. However, the procedures of matrix inversion usually are constructed formally thus special care should be taken in order not to lose in the basis set the appropriate corrections of the wave functions due to quadrupole and polarization effects and to the quadratic Stark effect, that were described earlier above. This way would need much more computational efforts and very often the basis set is intentionally cut by omission of the basis set corrections due to, for example, the quadratic Stark effect [61]. But as it was already stated here as well as in other works [46,48,53,56] the better agreement with experiment gained by such a procedure [49,61] is not more than an illusion created by nonconsistent accounting for the quadratic Stark effect corrections [64].

Nevertheless, discussed sources of discrepancy of the "bulk core of Stark profile" with respect to the HWHM and dip values and compared to ST profile [39,40], that in the frames of the simple model used here does not include asymmetry corrections, are quite clear and insignificant for the aims of the present paper. It should be also stressed that one should distinguish the results derived by the rigorous consistent theoretical formulation, and those that were obtained in addition by various fitting procedures in an attempt to make theoretical values better than they are in reality. One of the examples of such practice is the semiempirical cutoff procedure in the ST.

As about the difference with VCS, keeping aside asymmetry features and its mismatch with experimental values, it is connected with the employed in VCS the one electron approximation procedure for description of the transition between the impact and quasistatic regime of broadening by electrons versus increasing the detuning from the line center. It is seen that the realization of this transition, that also was constructed by hands to sew the one electron approximation with the impact limit, seems to underestimate the range of the validity of the impact approximation and thus leads to lesser HWHM and wing intensity.

The above analysis is illustrated by comparison performed in Fig. 7. In Fig. 7(a) these profiles are compared, while in Fig. 7(b) one can see deviations in the HWHM. It should be noted as well, that the parabolic individual impact widths give larger values of the impact broadening than spherical ones in ST. Although this fact is known since the work of [73] it was not systematically studied. The similar paradoxes were met recently in the other problem, analyzing the rates of cascade transitions for the dielectronic recombination in the electric field in the parabolic and spherical basis [82]. In a more general setting when the assumption of the density matrix diagonality is avoided, it is necessary to construct somehow the transition from population of levels in the $\{n\ell m\}$ space to $\{n_1 n_2 m\}$ one. This smooth transition versus the detuning from the line center is quite a complex problem, which is not resolved yet and needs to go beyond conventional setting of the broadening problem. In fact the proper setting is possible in the frames of kinetic theory of broadening by joining the balance and radiative coherence equations [79].

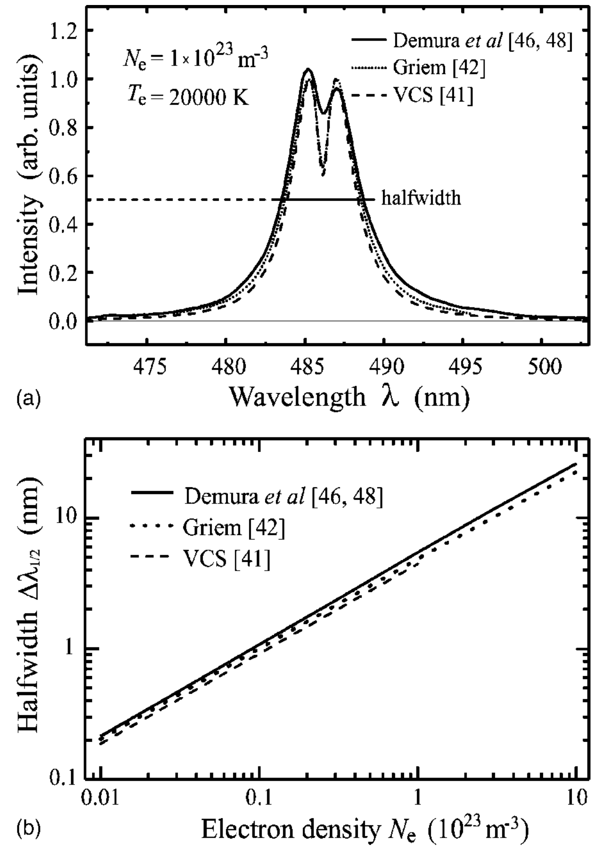

FIG. 7. (a) The comparison of H_β spectral line profiles predicted by different theoretical models. (b) The various theoretical dependencies of H_β halfwidth on the electron density.

V. COMPARISON OF EXPERIMENTAL AND THEORETICAL RESULTS

A. Parameter A_1

Figure 8(a) shows the comparison of the experimental values of asymmetry parameter A_1 in terms of the distance from the central line with the model results for the electron density of 7.30×10^{17} cm^{-3}. The distances from the central line $\Delta\lambda$, at which the asymmetry parameter A_1 is measured, are chosen to be approximately equal to the distances which correspond to the points at 0.8, 0.7,…, 0.1 of the maximal intensity I_0. The increase of the absolute values of the parameter A_1 versus the increase of $|\Delta\lambda|$ towards either smaller or larger wavelengths is clearly seen. For negative values, at the lowest measured detuning from the central line, the ratio $A_1^{(\mathrm{expt})}/A_1^{(\mathrm{theor})}$ is typically below 10.0, and for positive values at the highest detuning from the central line it is around 4. The experimental and theoretical curves should cross at the distance $\Delta\lambda=\Delta\lambda_{1/2}/2$ from the central line where $A_1=0$. The small deviations from this value arise due to an error introduced during the determination of the asymmetry parameter. The errors amount from ±5% up to ±19% for negative values, and ±6% up to ±20% for positive values of the asymmetry parameter A_1 depending on the electron density. The measurement errors are also indicated in Fig. 8.

B. Parameter A_2

The comparison of the experimental and theoretical values of the parameter A_2 is presented in the Fig. 8(b) versus the ratio I/I_0 with electron density and temperature as in the case of parameter A_1. It is clear, on the basis of the definition of the parameter A_2 that it vanishes at the half-intensity $I/I_0=0.5$. The measured positive values of the parameter A_2 are from 7.5 to 4.0 times higher than the theoretical values, while the negative ones are from 4.6 to 8.2 times higher with increase of electron density. For positive values of the asymmetry parameter A_2, the measurement errors are in the range

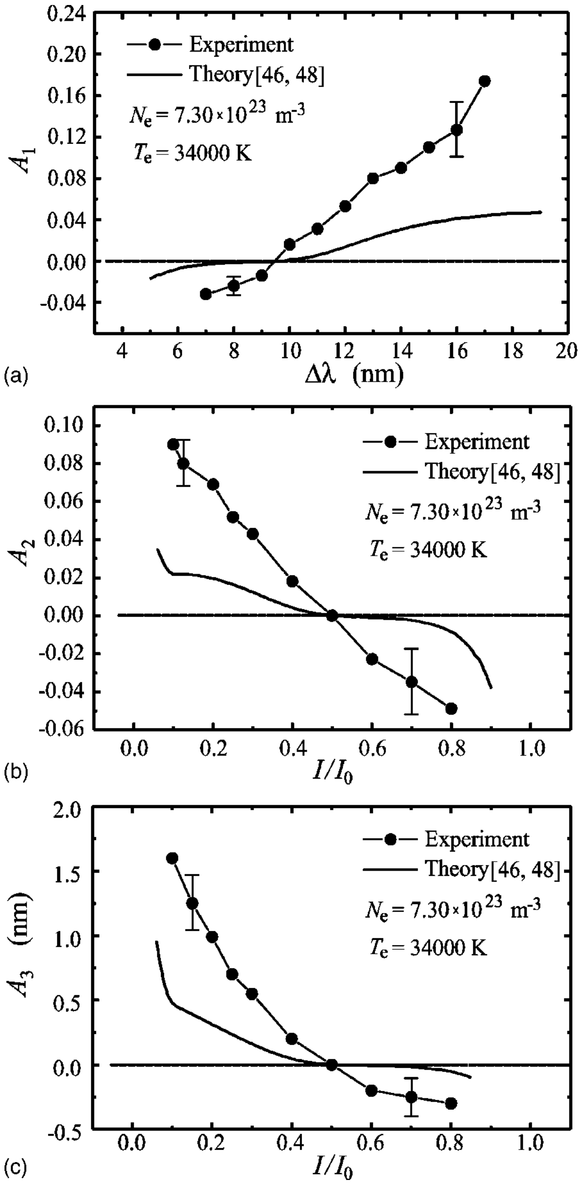

FIG. 8. The comparison of experimental and theoretical asymmetry parameters investigated in this work.

±5% to ±13%, and for the negative values these errors vary from ±10% to ±40%.

C. Parameter A_3

The comparison of experimental and theoretical values of the asymmetry parameter A_3 is presented in Fig. 8(c) in the same way as the values of the parameter A_2. The asymmetry parameter A_3 also vanishes for $I/I_0=0.5$. Although the experimental results show the similar behavior as the theoretical ones, the positive experimental values of the parameter A_3 are higher than the theoretical ones about 7.2 to 3.3 times, while the negative values are higher from 6.3 to 10.0 times with increase of electron density. The measurement errors for positive values of A_3 are in the range from ±5% to ±13% and for the negative values from ±10% to ±43%. It is clear that in the measurement of the very small values (close to zero) of all asymmetry parameters, introduced error is much higher and can reach even ±80%.

D. Discussion

Summarizing the results of comparison performed above (see Fig. 8) it is necessary to underline that the set of theoretical curves for each of the three asymmetry parameters have similar functional dependencies as experimental curves, thus demonstrating qualitative overall agreement in the main trends with suggested here the model description of the asymmetry in the whole Stark profile of H_β line. This encircles the expected behavior versus density and temperature. Although at the first sight (see Fig. 5), the complete experimental profile can be described rather well within the used theoretical model, the magnitude of the asymmetry in the model profiles is drastically lower than in the experimental ones. As it was noted above in the theoretical description applied here, the Holtsmark function was used for the ion microfield distribution function and the universal functions describing asymmetry are directly expressed through it [46,48]. These functions have much more flat "shoulders" and are wider than the corresponding functions accounting for the Debye screening by electrons and the ion-ion correlations [50–54]. That is why it may be expected that the inclusion in the scheme of the latter functions [50,51,53,54] which are narrower, steeper and have much higher maxima, would make the HWHM noticeably narrower while the behavior of asymmetry steeper at times, because the asymmetry functions contain the differentiation operation [50]. One also should take into account the polarization effects [50,51,53,54].

It should be separately underlined that the theoretical profile and asymmetry are calculated first in the natural scale for the theory representation, namely, versus the circular frequency of radiation or the detuning in the circular frequency scale. On the contrary, the natural scale in the experiment is the wavelength of radiation. The procedure of conversion from one scale to another deforms the symmetric profile and this asymmetry contribution due to the conversion from the circular frequency scale to the wavelength scale is also ascribed to trivial asymmetry. The characteristics of such "trivial asymmetry" depend on the shape function. For example, the asymmetry sign would be different for the Lorentz profile and the Holtsmark asymptotic profile. In the case of the calculations performed for H_β it occurs that the conversion operation drastically decreases the magnitude of asymmetry in the wavelength scale in comparison with the circular frequency scale [64].

It is conventional to ascribe also to trivial asymmetry the radiative rate (due to ω^4 factors) and the Boltzmann factor dependence on current frequency values in the contour [61], although in ST both these factors are dropped out [39,40]. The influence of these factors on asymmetry is opposite: the Boltzmann factor increases the red wing with respect to the blue one, while the ω^4 factor increases the blue wing. Although the exponential Boltzmann factor is a stronger function than the power function, the result of competition between two mechanisms depends on the line specifics (see

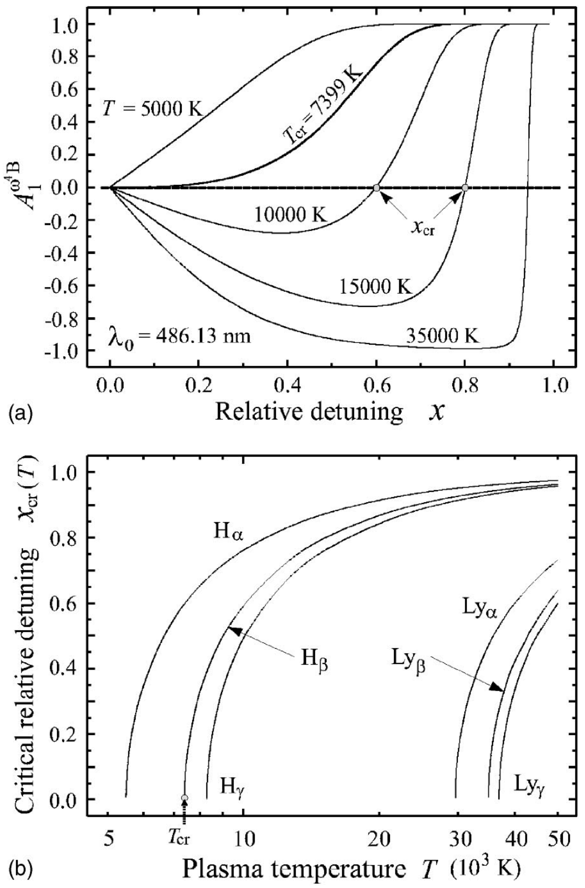

FIG. 9. (a) The additional contribution of Boltzmann and ω^4 factors to the asymmetry parameter A_1 in the case of H_β spectral line found for different plasma temperatures and wide range of relative detuning $x \equiv |\Delta\lambda|/\lambda_0$. (b) The illustration of how line specifics set the temperature dependence of critical relative detuning x_{cr} and define the values for critical temperature T_{cr} below which red asymmetry ($A_1^{\omega^4 B} > 0$) completely takes over.

Fig. 9). As Fig. 9(a) illustrates, in the case of H_β such competition may lead to red asymmetry ($A_1^{\omega^4 B} > 0$) for all relative detunings ($x \equiv |\Delta\lambda|/\lambda_0$) only if plasma temperature T is lower than certain critical temperature (T_{cr}=7399 K). The critical relative detuning x_{cr} for given plasma temperature $T > T_{cr}$ is defined as point in Fig. 9(a) at which the asymmetry parameter $A_1^{\omega^4 B}$ (originating solely due to Boltzmann and ω^4 factor) changes its sign. It is obvious from Fig. 9(b) that $x_{cr}=0$ defines critical plasma temperature T_{cr} which in turn strongly depends on the spectral line in question. However, there is a lot of controversy with the inclusion of these factors because in this case the possibility of normalization of the contour to unity becomes doubtful in the conventional setting when the upper and lower integration limits of $\Delta\omega$ could be put to $\pm\infty$ accordingly. The inclusion of those factors is possible only for the fixed spectra limits and in fact leads to the failure of the applicability of the conventional profile definition as it is. No words that for such an extremely wide line as H_β this problem has crucial importance. Moreover, the introduction of Boltzmann factors contradicts the fundamental assumption in the theory of broadening—the density matrix diagonality for the degenerate states with fixed principal quantum number, used conventionally in the derivation of the profile expression [64]. And at last, the test calculations for plasma temperatures found in this work [see Fig. 9(a)], reveal that the direct implementation of both factors in the line shape leads in the case of H_β to the strong blue asymmetry for all investigated values of detuning from the line center that evidently contradicts to experiment [64]. It is strange, that in other works on the subject the problems encountered here with the formal substitution of Boltzmann factors and ω^4 factor were not reported [61]. There is also another debatable consideration, in which these factors are attributed to the continuum, which would lead to the much larger experimental asymmetry and would overturn the current experimental methods of the experimental treatment. So, in view of all this controversy these factors are dropped again in the line shape expressions due to the absence at the moment of the consistent procedure of their consideration. Probably, the correct consideration of the inclusion of the mentioned factors into the asymmetry calculations should be performed together with the description of the electron broadening transition from the impact to the quasistatic regimes and simultaneously accounting for the polarization and quadrupole effects in the electron-radiator interaction.

The other concern is of the strong dependence of asymmetry on the values of the electronic impact shifts. In the earlier paper it was shown that the increase of the shifts by 1.5 times strongly influences the asymmetry behavior even qualitatively, depending on the choice of the reference point [64]. At the moment there is still a lot of controversy [83–87] in the calculations of the electron Stark shifts and further development in this field would give possibility to improve the asymmetry description. It should be noted, however, that in the cited works the shift of the "line gravity" is considered, contrary to the impact shifts of individual Stark components employed in the present work.

And the last concerns the further theory development in order to include the terms in the next order on the parameter ε. Here it would be appropriate to warn again against the inconsistent inclusion of only the quadratic Stark effect (QSE) shifts that leads to the illusive satisfactory agreement with experiment [49,61], as it was once more shown explicitly in [64].

In this context in the recent publication [63] it was attempted to address QSE with enlarged basis including quenching interaction with levels $n'=n\pm1$, $n\pm2$ in a somewhat artificial spherical basis. Indeed, it is known that namely these levels give the main contribution to QSE, but it happens in the parabolic basis, that in the spherical basis would either correspond to infinite sums. Thus it is unlikely that this method can reproduce well known results of QSE and therefore the benefits of its implementation seem doubtful. Besides that, as already was shown in [56], the results in [52] for the matrix elements of quadrupole interaction were obtained with arithmetical mistakes that entered in calculations in the further works (see for example [60,61]).

VI. CONCLUSIONS

The subject of this study is the asymmetry of the experimental profiles of H_β in T-tube plasmas for the wide range of electron densities and temperatures. Actually, the asymmetry of the complete profile except line peaks was considered. The results obtained are compared to the theoretical data [46,48]. The set of three asymmetry parameters is defined and both the experiment and the theoretical model [46,48] are described in detail. It is shown that the theoretical approach accounting for the microfield nonuniformity in the quasistatic approximation [46,48] and the electron impact shifts [59,60], provides qualitatively proper description of the shape of the experimental profile of H_β line obviously much better than ST and VCS [40,41]. However, it should be mentioned, that the implemented theoretical model [46,48] gives for the same linewidth about 15% lower electron density than ST. However, this is not astonishing since the deployed model uses the Holtsmark microfield distribution function, which is wider than the Hoopers distribution in ST. The special attention was paid during the experimental research in avoiding the appearance of possible trivial asymmetry sources. In order to analyze the profile of H_β line, three asymmetry parameters were investigated. The parameter A_1 describes the asymmetry in terms of spectral intensities of the blue and red parts of the line profile as the function of the distance from the central line, and the parameters A_2 and A_3 in terms of the distance from the central line as a function of the ratio of the spectral intensity at the measurement site and the maximal intensity. All three parameters indicate that experimental profiles have larger magnitude of asymmetry than the theoretical ones [46,48]. The form of the dependence, however, for all three asymmetry parameters is of the same type as the theory [46,48] predicts. The asymmetry of the profile of H_β line increases either towards longer or shorter wavelengths from the line center. The asymmetry also increases with increasing electron density. These data undoubtedly indicate that the asymmetry is the property of the complete H_β line profile, and not only of the clearly expressed blue and red maximum.

The intention of this work, besides the determination of the profile asymmetry, is to indicate also the necessity to use the whole profile of H_β line for the diagnostic purposes, and not to measure only the line halfwidth. The presented here theoretical description, based mainly on [46,48], indicates that such possibility with further improvement of the theoretical calculations can become a real option. The first step of refinement should account for the Debye electron screening, ion-ion correlation and polarization effects, which is currently feasible [53,54].

It is expected that presented above experimental data, benchmarked by the comparison with the transparent theoretical model, will serve for the further improvement of understanding and treating the Stark profiles asymmetry of hydrogen-like radiators in plasmas.

ACKNOWLEDGMENTS

The work of S. Djurović and D. Nikolić is supported by the Ministry of Science, Technology and Development of Republic of Serbia under project 1736. A. V. Demura wishes to thank Professor Marco Gigosos and Professor Manuel Gonzalez for instructive discussions on the trivial asymmetry, and Professor Volkmar Helbig for the earlier extensive collaboration on the subject at large, supported partly by DAAD, as well as Professor Sybille Günter for sending her Habilität dissertation. A. V. Demura also acknowledges support by Observatoire de Paris for a long period collaboration on the subject with Dr. Chantal Stehle and Dr. Nicole Feautrier, and by CEA for collaboration with Dr. Dominique Gilles.

[1] W. Finkelburg, Z. Phys. **70**, 375 (1931).
[2] G. Jürgens, Z. Phys. **134**, 21 (1952).
[3] M. Pavlov, Ph.D. thesis, University of Liverpool, 1968.
[4] W. L. Wiese, D. E. Kelleher, and D. R. Paquette, Phys. Rev. A **6**, 1132 (1972).
[5] D. D. Burgess and R. Mahon, J. Phys. B **5**, 1756 (1972).
[6] D. E. Kelleher and W. L. Wiese, Phys. Rev. Lett. **31**, 1431 (1973).
[7] W. L. Wiese, in *Physics of Ionized Gases*, edited by M. V. Kurepa, VI Yugoslav Symposium and Summer School on the Physics of Ionized Gases (SPIG VI) (Institute of Physics, Beograd, Yugoslavia, 1972), pp. 559–596.
[8] W. L. Wiese, in *Physics of Ionized Gases*, edited by V. Vujnović, VII Yugoslav Symposium and Summer School on the Physics of Ionized Gases (SPIG VII) (Institute of Physics, Zagreb, Yugoslavia, 1974), pp. 637–673.
[9] W. L. Wiese, D. E. Kelleher, and V. Helbig, Phys. Rev. A **11**, 1854 (1975).
[10] L. J. Roszman, Phys. Rev. Lett. **34**, 785 (1975).
[11] J. D. Hey and H. R. Griem, Phys. Rev. A **12**, 169 (1975).
[12] R. D. Bengtson and G. R. Chester, Phys. Rev. A **13**, 1762 (1976).
[13] R. C. Preston, J. Phys. B **10**, 523 (1977).
[14] D. E. Kelleher, N. Konjević, and W. L. Wiese, Phys. Rev. A **20**, 1195 (1979).
[15] H. Ehrich and D. E. Kelleher, Phys. Rev. A **21**, 319 (1980).
[16] C. Fleurier, G. Coulaud, P. Ranson, and J. Chapelle, Phys. Rev. A **21**, 851 (1980).
[17] V. Helbig and K. P. Nick, J. Phys. B **14**, 3573 (1981).
[18] M. Pavlov and S. Djurović, Review of Research: Phys. Ser. **12**, 43 (1982).
[19] F. Torres, M. A. Gigosos, and S. Mar, J. Quant. Spectrosc. Radiat. Transf. **31**, 265 (1984).
[20] S. R. Goode and J. P. Deavor, Spectrochim. Acta, Part B **39**, 813 (1984).
[21] S. Djurović and M. Pavlov, Beitr. Plasmaphys. **24**, 105 (1984).
[22] V. Radujkov and M. Pavlov, Review of Research: Phys. Ser. **15**, 41 (1985).
[23] M. Pavlov and V. Radujkov, J. Quant. Spectrosc. Radiat. Transf. **33**, 475 (1985).
[24] J. Halenka and J. Musielok, J. Quant. Spectrosc. Radiat. Transf. **36**, 233 (1986).

[25] M. Pavlov, Z. Mijatović, S. Djurović, and V. Radujkov, Review of Research: Phys. Ser. **16**, 53 (1986).
[26] C. Carlhoff, E. Krametz, J. H. Schäfer, and J. Uhlenbusch, J. Phys. B **19**, 2629 (1986).
[27] Z. Mijatović, M. Pavlov, and S. Djurović, J. Quant. Spectrosc. Radiat. Transf. **38**, 209 (1987).
[28] S. Djurović, Z. Mijatović, and R. Kobilarov, Contrib. Plasma Phys. **28**, 229 (1988).
[29] J. Halenka, J. Quant. Spectrosc. Radiat. Transf. **39**, 347 (1988).
[30] J. Halenka, B. Vujičić, and S. Djurović, J. Quant. Spectrosc. Radiat. Transf. **42**, 571 (1989).
[31] J. Uhlenbusch and W. Viöl, Contrib. Plasma Phys. **29**, 459 (1989).
[32] S.-K. Chan and A. Montaser, Spectrochim. Acta, Part B **44**, 175 (1989).
[33] Z. Mijatović, M. Pavlov, and S. Djurović, Phys. Rev. A **43**, 6095 (1991).
[34] C. Thonmsen and V. Helbig, Spectrochim. Acta, Part B **46**, 1215 (1991).
[35] I. Savić, B. Vujičić, S. Djurović, and M. Pavlov, in *Contributed Papers & Abstracts of invited lectures and Progress Reports*, edited by B. Vujičić and S. Djurović, XVIII Yugoslav Symposium and Summer School on the Physics of Ionized Gases (SPIG XVIII) (Institute of Physics, Novi Sad, Yugoslavia, 1996), pp. 294–297.
[36] S. Djurović, Z. Mijatović, M. Pavlov, R. Kobilarov, and B. T. Vujičić, Zh. Prikl. Spektrosk. **64**, 566 (1997) (in Russian).
[37] I. Savić, B. Vujičić, S. Djurović, and M. Pavlov, in *Contributed Papers & Abstracts of invited lectures and Progress Reports*, edited by N. Konjević, M. Ćuk, and I. R. Videnović, XIX Yugoslav Symposium and Summer School on the Physics of Ionized Gases (SPIG XIX) (Faculty of Physics, University of Belgrade, Belgrade, Yugoslavia, 1998), pp. 377–380.
[38] J. M. Luque, M. D. Calzada, and M. Sáez, J. Phys. B **36**, 1573 (2003).
[39] H. R. Griem, *Plasma Spectroscopy* (McGraw-Hill, New York, 1964).
[40] P. Kepple and H. R. Griem, Phys. Rev. **173**, 317 (1968).
[41] C. R. Vidal, J. Cooper, and E. W. Smith, Astrophys. J., Suppl. **25**, 37 (1973).
[42] H. R. Griem, *Spectral Line Broadening by Plasmas* (Academic, New York, 1974).
[43] M. A. Gigosos, M. A. González, and V. Cardeñoso, Spectrochim. Acta, Part B **58**, 1489 (2003).
[44] H. R. Griem, Z. Phys. **137**, 280 (1954).
[45] L. P. Kudrin and G. V. Sholin, Sov. Phys. Dokl. **7**, 1015 (1963).
[46] A. V. Demura and G. V. Sholin, J. Quant. Spectrosc. Radiat. Transf. **15**, 881 (1975).
[47] A. de Kertanguy, N. T. Minh, and N. Feautrier, J. Phys. B **12**, 365 (1979).
[48] A. Demura, V. V. Pleshakov, and G. V. Sholin, Preprint No. IAE-5349/6, I. V. Kurchatov Institute of Atomic Energy, Moscow, 1991, 98 p. (in Russian), translation to French by Dr. M. Busquet, 1993.
[49] R. F. Joyce, L. A. Woltz, and C. F. Hooper, Jr., Phys. Rev. A **35**, 2228 (1987).
[50] A. Demura, Preprint No. IAE-4632/6, I.V. Kurchatov Institute of Atomic Energy, Moscow, 1988, 17 p. (in Russian), translation to French by Dr. M. Busquet, 1993.
[51] A. V. Demura, in *Contributed Papers*, edited by J. Szudy, (Ossolineum, Wroclaw, Poland, 1989), pp. A39–A40 (ICSLS IX).
[52] J. Halenka, Z. Phys. D: At., Mol. Clusters **16**, 1 (1990).
[53] A. V. Demura and C. Stehlè, in *Spectral Line Shapes*, edited by A. D. May, J. R. Drummond, and E. Oks, AIP Conf. Proc. No. 328 (AIP, New York, 1995), pp. 177–208 (ICSLS XII).
[54] A. V. Demura, D. Gilles, and C. Stehlè, J. Quant. Spectrosc. Radiat. Transf. **54**, 123 (1995).
[55] A. V. Demura, D. Gilles, and C. Stehlè, in *Strongly Coupled Coulomb Systems*, edited by G. J. Kalman, K. Blagoev, and J. M. Rommel (Plenum, New York, 1998), pp. 377–380.
[56] C. Stehlè, D. Gilles, and A. V. Demura, Eur. Phys. J. D **12**, 355 (2000).
[57] A. V. Demura, D. Gilles, and C. Stehlè, in *Spectral Line Shapes*, edited by J. Seidel, AIP Conf. Proc. No. 559 (AIP, New York, 2001), pp. 99–107 (ICSLS XV).
[58] A. V. Demura and C. Stehlè, in *Spectral Line Shapes*, edited by J. Seidel, AIP Conf. Proc. No. 559 (AIP, New York, 2001), pp. 111–113 (ICSLS XV).
[59] L. Hitzschke, G. Ropke, T. Seifert, and R. Zimmermann, J. Phys. B **19**, 2443 (1986).
[60] A. Könies and S. Günter, J. Quant. Spectrosc. Radiat. Transf. **52**, 825 (1994).
[61] S. Günter and A. Könies, Phys. Rev. E **55**, 907 (1997).
[62] S. Sörge and S. Günter, Eur. Phys. J. D **12**, 369 (2000).
[63] W. Olchawa, J. Quant. Spectrosc. Radiat. Transf. **74**, 417 (2002).
[64] A. V. Demura, V. Helbig, and D. Nikolić, in *Spectral Line Shapes*, edited by C. A. Back, AIP Conf. Proc. No. 645 (AIP, New York, 2002), pp. 318–324 (ICSLS XVI).
[65] N. Hoe, B. D'Etat, J. Grumberg, M. Caby, E. Leboucher, and G. Coulaud, Phys. Rev. A **25**, 891 (1982).
[66] J. Holtsmark, Ann. Phys. **58**, 577 (1919).
[67] K. Grützmacher and B. Wende, Phys. Rev. A **16**, 243 (1977).
[68] A. C. Kolb, Phys. Rev. **107**, 345 (1957).
[69] M. Pavlov and A. N. Prasad, Z. Phys. **212**, 266 (1968).
[70] G. Boldt and W. S. Cooper, Z. Naturforsch. A **19a**, 968 (1964).
[71] I. Ishii, R. H. Clifford, A. Montaser, B. A. Palmer, and L. R. Lyman, *Measurement of Electron Number Density for Argon and Helium ICP Discharges by Using Various Hydrogen Lines*, presented at the 17th FACSS Meeting (Cleveland, OH, USA, 1990).
[72] A. Montaser and S.-K. Chan, SCAN, CONVERT and NE: New computer programs for the determination of electron number density via stark broadening, U. S. Copyright, Department of Chemistry, The George Washington University, Washington, DC, 20052, USA, 1989.
[73] G. V. Sholin, A. V. Demura, and V. S. Lisitsa, Sov. Phys. JETP **37**, 1057 (1973).
[74] N. Hoe, E. Banerjea, H. W. Drawin, and L. Herman, J. Quant. Spectrosc. Radiat. Transf. **5**, 835 (1965).
[75] H. R. Griem, Phys. Rev. A **27**, 2566 (1983).
[76] H. R. Griem, Phys. Rev. A **28**, 1596 (1983).
[77] H. R. Griem, Phys. Rev. A **38**, 2943 (1988).
[78] C. F. Hooper, Jr., Phys. Rev. **165**, 215 (1968).
[79] A. V. Anufrienko, A. E. Bulyshev, A. L. Godunov, A. V. Demura, Y. K. Zemtsov, V. S. Lisitsa, and A. N. Starostin, Sov. Phys. JETP **76**, 219 (1993).

[80] F. Khelfaoui, these, Univ. de Provence, 1991; B. Talin (private communication).
[81] S. Alexiou, in *Spectral Line Shapes*, edited by M. Zoppi and L. Ulivi AIP Conf. Proc. No. 386 (AIP, New York, 1997), pp. 79–98 (ICSLS XIII).
[82] V. S. Lisitsa (private communication).
[83] A. Escarguel, E. Oks, J. Richou, and D. Volodko, Phys. Rev. E **62**, 2667 (2000).
[84] H. R. Griem, Phys. Rev. E **64**, 058401 (2001).
[85] E. Oks, J. Phys. B **35**, 2251 (2002).
[86] J. Halenka, Phys. Rev. E **69**, 028401 (2004).
[87] E. Oks, Phys. Rev. E **69**, 028402 (2004).